ARTICLE

Self-Assembly of Heterogeneously Charged Particles under Confinement

Emanuela Bianchi,[†,*] Christos N. Likos,[‡] and Gerhard Kahl[†]

[†]Institut für Theoretische Physik and Center for Computational Materials Science (CMS), Technische Universität Wien, Wiedner Hauptstrasse 8-10, A-1040 Vienna, Austria, and [‡]Faculty of Physics, University of Vienna, Boltzmanngasse 5, A-1090 Vienna, Austria

ABSTRACT Self-assembly—the spontaneous organization of microscopic units into well-defined mesoscopic structures—is a fundamental mechanism for a broad variety of nanotechnology applications in material science. The central role played by the anisotropy resulting from asymmetric shapes of the units and/or well-defined bonding sites on the particle surface has been widely investigated, highlighting the importance of properly designing the constituent entities in order to control the resulting mesoscopic structures. Anisotropy driven self-assembly can also result from the multipolar interactions characterizing many naturally occurring systems, such as proteins and viral capsids, as well as experimentally synthesized colloidal particles. Heterogeneously charged particles represent a class of multipolar units that are characterized by a competitive interplay between anisotropic attractive and repulsive interactions, due to the repulsion/attraction between charged-like/oppositely charged regions on the particle surface. In the present work, axially symmetric quadrupolar colloids are considered in a confined planar geometry; the role of both the overall particle charge and the patch extension as well as the effect of the substrate charge are studied in thermodynamic conditions such that the formation of extended structures is favored. A general tendency to form quasi-two-dimensional aggregates where particles align their symmetry axes within the plane is observed; among these planar self-assembled scenarios, a clear distinction between the formation of microcrystalline gels—branched networks consisting of purely crystalline domains—as opposed to disordered aggregates can be observed based on the specific features of the particle−particle interaction. Additionally, the possible competition of interparticle and particle−substrate interactions affects the size and the internal structure of the aggregates and can possibly inhibit the aggregation process.

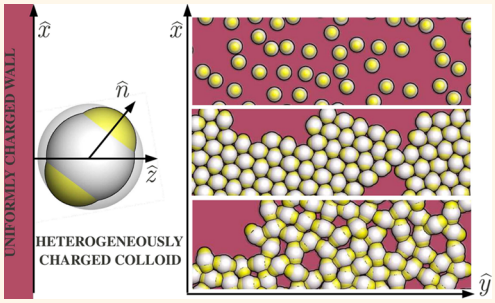

KEYWORDS: inverse patchy colloids · heterogeneously charged particles · self-assembly · microcrystalline gels · charged substrates · quasi-two-dimensional confinement

A broad range of self-organizing systems such as viruses, proteins, and clays are known to give rise to a wealth of structures by virtue of the asymmetry in their shapes and/or in their interaction surface patterns. Viruses and virus-like nanoparticles[1,2] used for the production of photonic crystals with a broad range of optical applications,[3] S-layer proteins that self-organize into highly symmetric planar lattices with well-defined pores,[4] and industrial synthetic clays forming stable gel phases at extremely low densities[5] are just few of the most recent examples of anisotropy driven self-assembly. In the realm of synthesized nano- and microsized colloids, new classes of mesoscopic particles with specific, nonspherical shapes[6] and colloidal particles with chemically or physically patterned surfaces, known as "patchy particles",[7−9] are regarded as novel building blocks for a new generation of smart materials with specific symmetries and physical properties.[10−14]

The previous examples provide evidence that anisotropic particle−particle interactions can originate from nonspherical shapes and/or from surface moieties. Over the past decade, investigations have focused on the possibilities offered to the self-assembly by asymmetric shapes, such as ellipsoids, discs, and polyhedra,[11,12,15] and/or by the presence of a small number of attractive regions, termed patches, on the surface of otherwise repulsive colloids;[7−9] in the latter case, the orientational and possibly selective bonding mechanism mediated by the patches guarantees a fine control over the features of the equilibrium, ordered as well as disordered, self-assembled structures.[13,16]

An additional and ubiquitous source of anisotropy at the level of particle−particle interactions is charge heterogeneity. When dispersed in a microscopic medium, colloids can acquire charge due to dissociation of surface groups and/or preferential adsorption

* Address correspondence to emanuela.bianchi@tuwien.ac.at.

Received for review March 26, 2013 and accepted April 29, 2013.

Published online April 29, 2013
10.1021/nn401487m

of charged species; the resulting, possibly inhomogeneous, surface charge distribution leads to strong multipolar interactions, which can significantly affect the self-organization of particles into specific structures.[5] Moreover, also naturally occurring systems such as proteins and virus capsids are known to have heterogeneously charged surfaces which give rise to specific collective behaviors.[1,4,17,18]

Heterogeneously charged particles can be generally regarded as charged patchy colloids. To emphasize that these systems significantly differ from conventional patchy colloids, we have termed them *inverse patchy colloids* (IPC);[19] "inverse" refers to the fact that, while conventional patchy systems are typically characterized by the presence of attractive regions on the surface of otherwise repulsive particles,[7,8] inverse patchy colloids carry extended patches that repel each other and attract those parts of the colloid that are free of patches. Due to the repulsion between like-charge regions and the attraction between oppositely charged regions, the effective interaction between heterogeneously charged units can be both attractive and repulsive, depending on the relative orientation of the particles.

For IPC systems, the Debye–Hückel theory, traditionally used to describe the electrostatic interactions between homogeneously charged colloids in a dielectric medium,[20] can be generalized to properly account for the effects of charge heterogeneity. Recently, we have put forward such a general approach that bridges the gap between a microscopic and a mesoscopic, coarse-grained description of IPCs.[19] In particular, we have designed a coarse-grained model for spherical colloids with an axially symmetric surface charge distribution due to the presence of two polar patches of the same charge, Z_p, and an equatorial region of opposite charge, Z_c. Our coarse-grained model reproduces the three-region particle surface and has three independent sets of parameters: the interaction range and strengths, which reflect the screening conditions and the ratio Z_p/Z_c, respectively, and the patch surface coverage.[19] For the present contribution, we considered IPCs under moderate screening conditions; that is, we fixed the particle–particle interaction range, δ, to 40% of the particle radius, σ, while we varied as free parameters (i) the patch surface extension (specified by the opening angle γ) and (ii) the overall particle charge, which was allowed both to vanish (neutral case) or differ from zero (overall charged cases). Details of how these parameters enter the modeling are summarized in the Model and Methods section (see also panels a and b of Figure 1). The overall particle charge affects the ratio of the directional attractive and repulsive contributions to the effective interactions; the same effect has also been reported in a recently proposed and related model.[21]

We investigated the self-organization scenarios of the selected IPC systems in a restricted geometry, confining the particles between two parallel, possibly

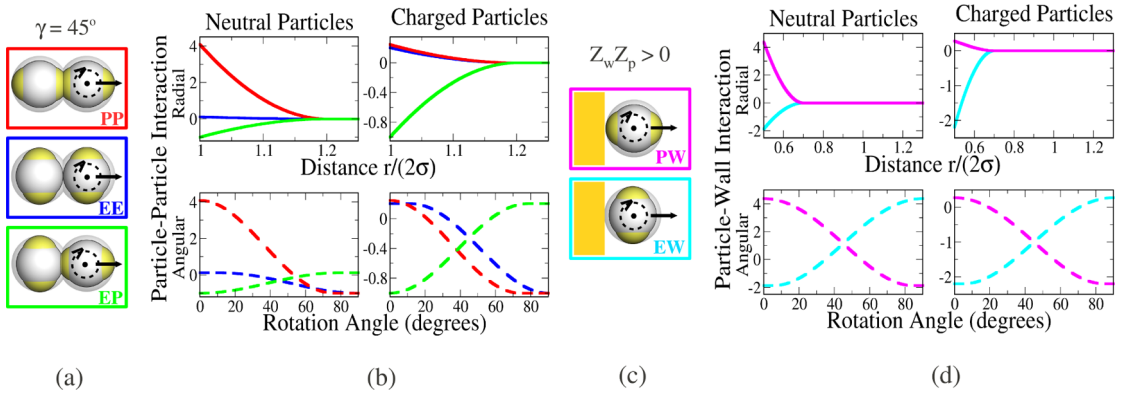

Figure 1. (a,b) Representation of the coarse-grained particle–particle interaction for both overall neutral and overall charged IPCs with patch extension γ = 45°. (a) Three characteristic particle–particle orientations for two IPCs at contact ($r = 2\sigma$), namely, the polar–polar (PP), the equatorial–equatorial (EE), and the equatorial–polar (EP) configurations. The coarse-grained IPC is composed by a gray central sphere, corresponding to the hard colloid; the two yellow caps represent the interaction spheres of the polar patches; the light gray halo around the central sphere features the interaction range of the bare colloid.[19] In each particle–particle configuration, the continuous black arrows indicate the translation direction of one IPC with respect to the other, while the dashed circles with one central dot represent the rotation of one IPC around an axis perpendicular to the plane. In the two top/bottom graphs of panel (b), the radial/angular dependence of the particle–particle interaction between two IPCs in the three selected configurations is shown; the red, blue, and green continuous/dashed lines correspond to different initial configurations: colloids at contact with PP, EE, and EP reciprocal orientation, respectively. (c,d) Representation of the coarse-grained particle–wall interaction between the selected IPC types and a planar wall with surface charge of the same sign as the patches, *i.e.*, $Z_wZ_p > 0$; the wall is reproduced in dark yellow on the left side with respect to the IPC. (c) Two characteristic particle–wall orientations for an IPC at distance $r = \sigma$ from the wall, namely, the polar–wall (PW) and the equatorial–wall (EW) configurations. Continuous arrows and dashed circles represent, respectively, the translational and rotational moves of the IPC with respect to the wall. In the two top/bottom graphs of panel (d), the radial/angular dependence of the particle–wall interaction is shown; the magenta and the turquoise continuous/dashed lines correspond to different initial configurations: colloid at contact with the wall in the PW and EW orientation, respectively. Table 1 reports the typical particle–particle and particle–wall minimum/maximum contact energies for each IPC type and each selected wall charge.

charged, horizontal walls. To this purpose, the particle−wall interactions were modeled consistently with the particle−particle interactions; the details of the modeling are described in the Model and Methods section (see also panels c and d of Figure 1). We considered both tight confinement conditions, such that the wall separation prevents particles from sitting on top of each other, and loose confinement conditions, which allow two particles to possibly assemble along the vertical direction. Our decision to study the self-assembly in a confined geometry was motivated by the fact that such quasi-two-dimensional setups are amenable to an experimental realization[22] or can be assimilated to situations in which particles sediment onto a horizontal substrate with a chemically controlled surface charge.

The main focus of our investigation lies on exploring the conditions under which ordered *versus* disordered structures are favored. Controlling crystal *versus* gel formation is indeed an important issue in soft matter systems, where the interplay between, for example, spherical/localized or specific/nonspecific interactions can favor the formation of either disordered aggregates or crystalline domains.[23,24] For the investigated IPC systems, a sharp distinction between two different scenarios occurs: the formation of disordered gel-like structures, characterized by a large fraction of local, ring-like arrangements, and the self-assembly of microcrystalline domains with triangular particle coordinations, which themselves represent the branches of a disordered network. We refer to this latter scenario as microcrystalline gel. The parameter space was spanned by (i) the patch extension, (ii) the charge of the bottom wall, and (iii) the overall charge of the particle. In systems confined between neutral walls, the patch extension uniquely determines the internal structure of the aggregates, whereas the overall charge of the particles plays a minor role. In the cases of charged substrate, the extent of the domains (from extended aggregates to possibly monomers) was shown to be controlled by the wall charge, Z_w, for both the self-assembly scenarios identified in our investigation.

From the point of view of the multipole expansion of localized charge distributions, the IPCs considered in this work represent axially symmetric quadrupoles. While the self-assembly of dipolar colloids has been widely investigated,[25−28] the collective behavior of multipolar particles has received less attention so far,[25,29] despite the fact that heterogeneously charged, multipolar particles are abundant in nature as well as in many colloidal systems of new generation.[8] Contrary to many recent investigations which focused on the aggregation behavior of dipolar as well as multipolar particles in quasi-two-dimensional systems,[26,27,29] no field-induced self-assembly has been considered here for IPCs.

RESULTS AND DISCUSSION

Our discussion first focuses on a qualitative, visual analysis of the systems, attempting to understand the emerging morphologies of the self-assembled structures on energetic arguments; subsequently, we provide a more quantitative analysis of the characteristic features of the aggregates observed in the investigated systems.

A first indication about the self-assembly of IPCs into extended structures can be inferred by looking at typical simulation snapshots. Figure 2 provides an overview of all of the investigated systems confined between two planar walls separated by a distance such that the particles are prevented from sitting on top of each other; in the central column of the figure, systems confined between two neutral walls are depicted, while the left/right columns reproduce the corresponding cases in the presence of a charged bottom wall; the color code of the particles highlights the number of bonded interactions per IPC, which is defined as the number of particle−particle interactions with a negative pair energy.

Ordered *versus* Disordered Aggregates between Neutral Walls. For systems confined between neutral walls, the size and the internal structure of the aggregates formed by the particles is controlled exclusively by the

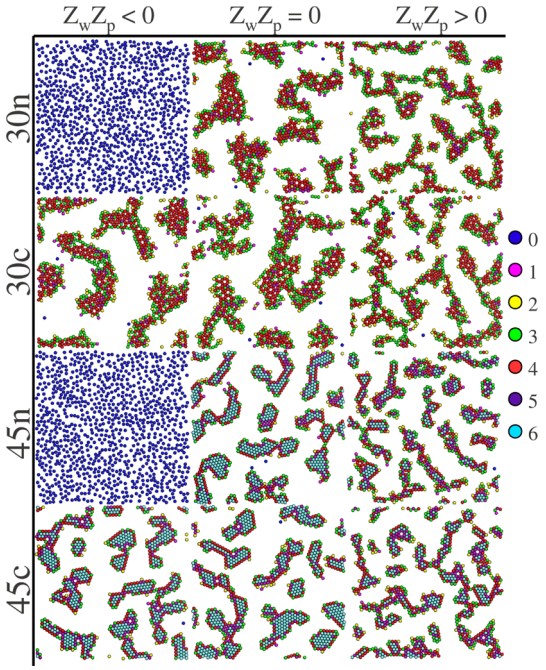

Figure 2. Top views of typical simulation snapshots of all the investigated IPC-types, labeled (from the top to the bottom) as 30n, 30c, 45n, and 45c, specifying both the patch size as well as the overall particle charge, under tight confinement between two parallel walls; while the top wall is always neutral, the bottom wall can be either neutral (panels in the central column) as well as charged (panels in the left and right columns). Colors represent the number of bonded interactions per particle; the color code is displayed on the right-hand side of the figure.

features of the pair potential, namely, the patch extension and the overall particle charge. The patch size is found to have a substantial influence on the morphology of the aggregates: while IPCs with smaller patches assemble into a locally and globally disordered gel structure, IPCs with bigger patches form a particle network whose branches are crystalline domains. Despite the absence of long-range order, the microcrystalline gel network shows a local triangular order due to the crystalline domains that constitute the gel branches. It is worth noting that the self-assembled network is either microcrystalline or disordered; that is, locally disordered domains and triangular crystalline domains do not occur in the same system. In contrast to conventional patchy systems, in IPC systems, larger patches favor the emergence of local spatial order. Surprisingly, the effect of the overall particle charge on the self-assembly process is found to be negligible: the visual analysis of overall charged particle systems indicates no significant differences, neither in the size nor in the morphology of the aggregates in comparison to the overall neutral particle systems. In conclusion, for systems confined between neutral walls, the tendency to self-assemble either into disordered or into ordered domains is mainly controlled by the size of the patch, while the overall charge of the particles and the ensuing different interplay between attractive and repulsive interactions play a minor role.

A quantitative analysis of the local surroundings of the particles is visualized by the color code of the snapshots displayed in Figure 2. Most of the particles in the disordered gel network form four bonds, corresponding to a bonding energy $u_{pb} \approx -1.6$ (in our reduced units), irrespective of the overall particle charge; in contrast, within the triangular domains of the microcystalline structure, the average number of bonds per particle is six, corresponding to a bonding energy $u_{pb} \approx -2.0$ (in our reduced units), for both the overall neutral and charged particle cases. Figure 3 clarifies in magnified views the local spatial structure of the typical aggregate morphologies: while systems with relatively big patches self-assemble into compact domains with a triangular particle arrangement, IPCs with smaller patches aggregate into a open gel network, where particles possibly arrange into ring-like structures, preferentially formed by five or six particles.

Effect of a Charged Plane on the Aggregation Process. As discussed above, for systems confined between two neutral walls, the size and the morphology of the aggregates depend only on the specific particle−particle interactions; consequently, the spatial orientation of particles forming dimers, trimers, and more extended aggregates is controlled by the features of the pair potential, while the orientation of isolated particles is homogeneous. When only monomers are considered, the presence of a charged plane at the bottom of the sample has intuitive effects: if the charges of the bottom wall and the patches have opposite sign (*i.e.*, $Z_w Z_p < 0$), the energetically preferred orientation of the particles is perpendicular to the *xy* plane (polar orientation, labeled PW in panel c of Figure 1); if the charges of the bottom wall and the patches have the same sign (*i.e.*, $Z_w Z_p > 0$), isolated particles prefer to orient themselves parallel to the *xy* plane (equatorial orientation, labeled EW in panel c of Figure 1). In contrast, when particles in clusters are considered, their orientation in space is the result of the competition between the particle−particle and particle−wall interactions; that is, the morphology of the aggregates depends on the balance between the average bonding energy of a particle with its neighbors, u_{pb}, and the bonding energy of a particle with its charged substrate, u_{wb}. For the chosen values of the wall charge, different scenarios take place, as described in what follows.

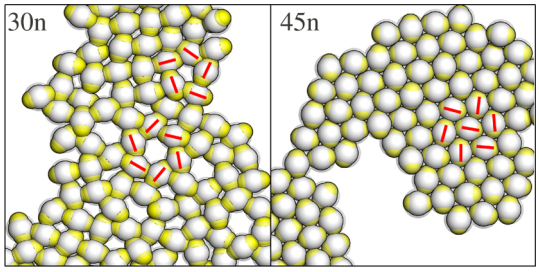

Figure 3. Magnified views of simulation snapshots of typical aggregates of overall neutral IPCs, labeled as 30n (left panel) and 45n (right panel), under tight confinement between two neutral walls. The local spatial order is highlighted by red bars indicating the orientation of the corresponding particle: IPCs with relatively small patches aggregate into disordered structures, possibly forming local ring-like arrangement of preferentially five or six particles; IPCs with relatively big patches self-assemble into ordered triangular domains.

When $Z_w Z_p < 0$, different behaviors were observed according to the overall charge of the particles: irrespective of their patch size, overall neutral particles do not self-assemble into extended structures, while overall charged particles form a disordered gel network similar to the corresponding one in the presence of a neutral bottom wall. In the cases of overall neutral particles, the energy gain in a particle orientation perpendicular to the *xy* plane is significantly bigger than the interparticle bonding energy (*i.e.*, $u_{pb}/u_{wb} \ll 1$). Particles therefore tend to approach each other with a relative orientation such that their equators face each other (EE configuration, reproduced in panel a of Figure 1) and consequently the strong particle−particle repulsion prevents bond formation. The aggregation process is thus completely inhibited, that is, the systems consist of monomers, as shown in Figure 2. In the overall charged cases, the energy gain of a particle−wall bond is negligible compared to the energy gain due to interparticle bonds (*i.e.*, $u_{pb}/u_{wb} \gg 1$). As a consequence, the aggregation process is essentially unaffected by the presence of the charged wall, as qualitatively shown in Figure 2.

When $Z_wZ_p > 0$, particles prefer to orient themselves parallel to the *xy* plane and hence planar aggregates, similar to the ones self-assembling between neutral walls, are expected to be favored. Nonetheless, irrespective of the essential features of the particle−particle interactions, the aggregation into large domains turned out to be less efficient compared to the formation of extended structures in the presence of neutral walls: as shown in Figure 2, the aggregates are significantly smaller and more elongated (*i.e.*, thinner). This striking difference is the result of a newly emerging competition: on one side, the interparticle bond formation favors a slightly nonplanar orientation of the particles, on the other side, the minimization of particle−wall interaction occurs when particles are parallel to the *xy* plane. Since in these systems $u_{pb}/u_{wb} \approx 1$, IPCs equally bond to their neighbors as well as to the bottom substrate; thus local particle rearrangements to optimize interparticle bonding may not occur efficiently. It is also worth noting that, while for IPCs with relatively small patches the internal structure of the aggregates is not significantly affected by the presence of the charged substrate, for IPCs with relatively big patches, the substrate influences the local spatial order of the self-assembled structures. In these latter cases, the presence of both triangular and locally disordered domains can be observed within the branches of the same gel network.

Size of the Aggregates. To quantify the size and the morphology of the emerging self-assembled structures, we have evaluated the pair correlation functions (plotted in panels a and b of Figure 4) that provide very clear information about the features of the observed aggregates. While overall neutral particles close to a charged bottom wall with $Z_wZ_p < 0$ are characterized by a fluid-like $g(r)$ which rapidly approaches to the ideal gas limit, in all other systems, the pair correlation functions are characterized by sharp peaks that signal the presence of strong correlations. The fast and often abrupt decay of these peaks suggests that the local correlations have a well-defined and rather short range, beyond which the system becomes homogeneous; the correlation range can thus be considered as a measure of the average size of the aggregates.[30] In order to extract this range from the $g(r)$, we defined a threshold value, h, and we calculated the maximum interparticle distance, r_h^{max}, at which the oscillations of $|g(r) - 1|$ reach that chosen value,[31] $|g(r_h^{max}) - 1| \equiv h$.

In panel c of Figure 4, r_h^{max} as a function of the wall charge is plotted for $h = 0.15$. A general trend can be observed for all of the cases in which aggregation occurs (*i.e.*, $r_h^{max} > 2\sigma$): under similar confinement conditions (*i.e.*, for a given sign of Z_wZ_p), bigger patches favor larger domains. Moreover, at fixed Z_wZ_p values, the domain size of the aggregates formed by IPCs with relatively small patches is insensitive to the overall charge of the particles; in contrast for IPCs with bigger

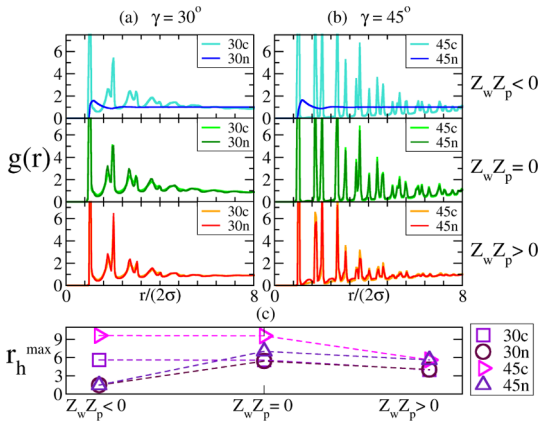

Figure 4. Top: radial distribution functions $g(r)$ for IPC systems with relatively small (a) and big (b) patches in different confinement conditions (*i.e.*, different values of Z_wZ_p). Results obtained for different choices of the overall particle charge are shown with different line colors (as labeled). Bottom: estimate of the aggregate size, r_h^{max} (as defined in the text), as a function of the surface charge of the bottom wall (c) for the four investigated combinations of patch size and overall particle charge (as labeled).

patches, overall charged particles self-assemble into domains that are often larger than those formed by their overall neutral counterparts. Additionally, for each IPC system, r_h^{max} assumes its maximum value when $Z_wZ_p = 0$. The maximum value of r_h^{max} also occurs in overall charged IPC systems when $Z_wZ_p < 0$, while the corresponding overall neutral cases under the same confinement conditions are characterized by $r_h^{max} \approx 2\sigma$ (*i.e.*, gas of monomers). Finally, when $Z_wZ_p > 0$, aggregates are smaller when compared to the corresponding ones formed between neutral walls; as pointed out before, in these cases, the observed reduced efficiency of the self-assembly process is due to the frustration of the preferred bond orientations.

Spatial and Orientational Order of the Aggregates. The analysis of the pair correlation functions also provides important information about the internal structure of the aggregates. Indeed, on the basis of the features of the $g(r)$, it is possible to distinguish between triangular and less ordered domains. When $Z_wZ_p = 0$, IPCs with relatively big patches form triangular crystalline domains, independently of the overall particle charge. In this case, the peaks in the $g(r)$ are sharply centered at $r/2\sigma = 1, \sqrt{3}, 1 + \sqrt{3}, 2,...$, and the $g(r)$ essentially vanishes between the first peaks. In contrast, under the same confinement conditions, IPCs with relatively smaller patches form disordered aggregates: the peaks in the $g(r)$ are smoother, their positions do not support a triangular order, and the minima of the $g(r)$ between the first peaks never approach to zero. The situation is more diversified for all of the cases in which, when $Z_wZ_p \neq 0$, the formation of extended aggregates occurs: while for IPCs with smaller patches, a charged bottom wall affects the local particle arrangement only to a minor extent, the charged wall can have a

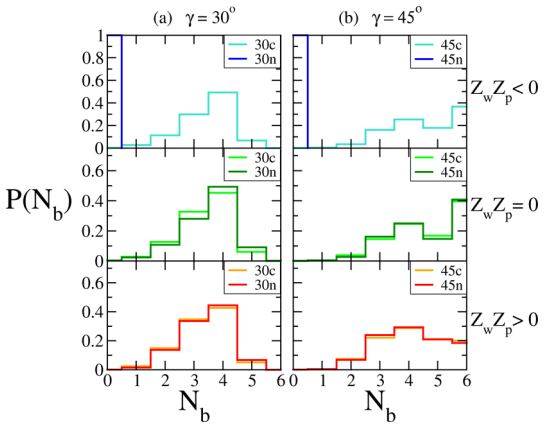

Figure 5. Histograms of the probability for a particle to have N_b bonds, $P(N_b)$. IPC systems with relatively small and big patches in different confinement conditions (*i.e.*, different Z_wZ_p values) are shown in panels a and b, respectively.

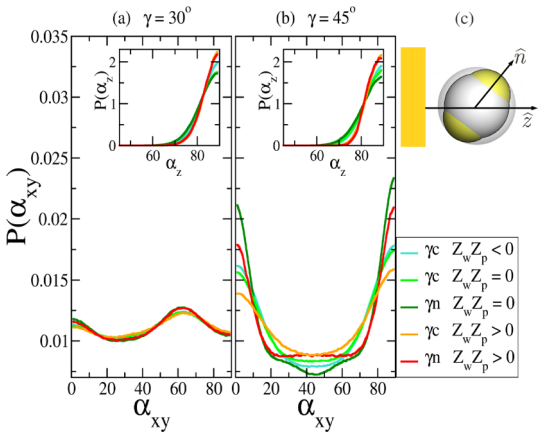

Figure 6. Orientational distributions $P(\alpha_{xy})$ and $P(\alpha_z)$ as functions of α_{xy} and α_z, respectively, calculated for bonded IPCs in their typical bonding environment, *i.e.*, $N_b = 4$ for IPCs with relatively small patches (a) and $N_b = 6$ for IPCs with relatively big patches (b). (c) Coarse-grained IPC close to the substrate is reproduced with its orientational vector $\hat{n}$. The main panels show the probability distributions of the angle between the projections on the *xy* plane of the orientational vectors of two neighboring particles, $P(\alpha_{xy})$; the insets display the probability distributions of the angle between the orientational vector of a particle and the *z*-axis, $P(\alpha_z)$. Curves corresponding to different cases are specified by different colors (as labeled).

significant effect on the local order within aggregates formed by IPCs with bigger patches. Indeed, when the latter systems are exposed to a charged substrate such that $Z_wZ_p > 0$, not only the main peaks of the $g(r)$ due to the triangular arrangement appear but also secondary peaks develop, indicating that, on average, the nearest neighbor order is not purely triangular. Such features of the $g(r)$ confirm the predominance of thin, elongated clusters where few ordered aggregates coexist with disordered domains within the same gel branches.

To gain a better insight on the morphology of the aggregates, we also calculated the probability for a particle to form N_b bonds, $P(N_b)$. Figure 5 reports the histograms of $P(N_b)$ for all of the studied cases. When $Z_wZ_p < 0$, aggregation of overall neutral particles is inhibited, that is, $P(N_b = 0) = 1$ (see the two corresponding panels of Figure 5). In all other cases, aggregation occurs and the corresponding $P(N_b)$ histograms show preferential values for N_b. As the existence and the position of a single pronounced peak indicates, IPCs with relatively small patches self-assemble into extended structures where most of the particles form four bonds, independently of the overall particle and wall charges (see left panels in Figure 5). In contrast, IPCs with relatively big patches assemble into aggregates where most of the particles form either four or six bonds (see right panels in Figure 5). More specifically, when $Z_wZ_p = 0$, the $P(N_b)$ histograms for systems of IPCs with relatively big patches are characterized by two peaks, independently on the overall particle charge: the higher peak at $N_b = 6$ is due to the particles in the bulk of the triangular clusters, and the lower peak at $N_b = 4$ is due to the particles on the boundaries of the aggregates; a very similar shape of the $P(N_b)$ histogram can be observed for overall charged IPCs when $Z_wZ_p < 0$. In contrast, when $Z_wZ_p > 0$, only one peak, centered at $N_b = 4$, can instead be observed irrespective of the overall particle charge: the number of particles forming six bonds is smaller than the number of particles with four bonds. This significant difference with respect to the other cases is related to (i) the presence of particle domains with nonperfect triangular arrangement within the gel network, and (ii) the predominance of the boundary regions over the bulk, due to smaller and more elongated clusters.

Finally, we characterized the orientational order within the aggregates *via* two different angles: the angle α_z between the particle orientational vector (see panel c of Figure 6) and the *z*-axis, and the angle α_{xy} between the projections on the *xy* plane of the orientational vectors of two neighboring particles. For this purpose, we classified the particles according to their number of bonds, N_b, and calculated the corresponding probability distributions, $P(\alpha_z)$ and $P(\alpha_{xy})$, for each type of bonded particles. Figure 6 reports $P(\alpha_z)$ and $P(\alpha_{xy})$ for bonded particles in their typical bonding environment, that is, $N_b = 4$ for IPCs with relatively small patches and $N_b = 6$ for IPCs with relatively big patches. Of course, systems that do not aggregate are not represented. For all of the investigated cases, the probability distributions $P(\alpha_z)$ are very similar to each other, suggesting that, regardless of the charge of the substrate, all types of IPCs in a highly bonded state tend orient themselves parallel to the *xy* plane (*i.e.*, $\alpha_z \approx 70-90°$). It is worth noting that, when $Z_wZ_p > 0$, planar particle orientations are favored and hence the corresponding $P(\alpha_z)$ curves are slightly more peaked at $\alpha \approx 90°$. The probability distributions $P(\alpha_{xyz})$ provide evidence of the presence of well-defined and distinct orientational ordering within the aggregates.

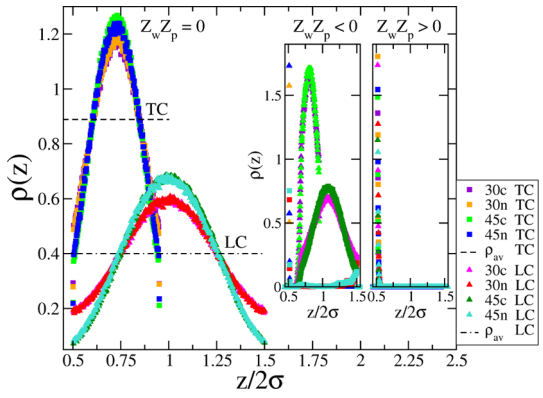

Figure 7. Density profiles $\rho(z)$ of the investigated IPC systems both under tight (TC) and in loose (LC) confinement as function of z (measured from the bottom plane). Main panel: density profiles when $Z_wZ_p = 0$; the dashed and dotted lines indicate the average number density, ρ_{av}, for tight and loose confinement, respectively. Insets: density profiles when $Z_wZ_p < 0$ (left) and $Z_wZ_p > 0$ (right). Profiles corresponding to different cases are specified by different symbols (as labeled).

In IPCs with relatively small patches, the $P(\alpha_{xy})$ curves deviate weakly from a homogeneous distribution; however, the presence of two smooth peaks, one at $\alpha_{xy} \approx 0$ the other at $\alpha_{xy} \approx 60°$, indicates a predominance of hexagonal ring structures (see also Figure 3). In contrast for IPCs with big patches, the $P(\alpha_{xy})$ curves are sharply peaked at $\alpha_{xy} \approx 0°$ and $\alpha_{xy} \approx 90°$ and show a more pronounced dependence on the system parameters. The maxima of the $P(\alpha_{xy})$ curves for IPCs with bigger patches indicate that particles orient themselves either parallel or perpendicular to their nearest neighbors (see also Figure 3). In these cases, the shape of the probability distributions slightly depends on the overall charge of the particles.

Effect of the Confinement. So far, we considered confinement conditions such that the distance between the walls prevented particles from sitting on top of each other (tight confinement). However and surprisingly, similar tendencies of IPCs to form planar structures were also observed under confinement conditions that allow particles to aggregate—in principle—along the z-axis (loose confinement). To quantitatively describe the particle distribution along the z-axis for the two different types of confinement, the density profiles, $\rho(z)$, have been evaluated. The density profiles of IPCs under tight confinement between neutral walls, shown in the main panel of Figure 7, are symmetric with respect to $z \approx L_z/2 = 0.725$ (in units of 2σ), confirming that all IPC systems under tight confinement self-assemble into essentially planar structures. Surprisingly, also systems under loose confinement between neutral walls form quasi-two-dimensional planes: the $\rho(z)$ curves are symmetric with respect to $z \approx L_z/2 = 1$ (in units of 2σ), as shown in the main panel of Figure 7. To summarize, when confined between neutral walls, all of the investigated IPC systems tend to self-assemble into almost planar structures, even when confinement conditions allow for the formation of nonplanar aggregates. It is worth noting that in both confinement types more pronounced peaks of the $\rho(z)$ curves correspond to IPCs with relatively bigger patches, indicating an enhanced propensity to form planar structures.

The similarities between systems under tight and under loose confinement continue to occur also when $Z_wZ_p \neq 0$, as shown in the insets of Figure 7. It is interesting to note that, when $Z_wZ_p > 0$, the density profiles are extremely peaked at $z/2\sigma = 0.5$ irrespective of the system parameters and of the confinement type; this means that the aggregation process occurs at the bottom wall; that is, particles form bonds with the substrate as well as with each other. In contrast, when $Z_wZ_p < 0$, the peaked density profiles at $z/2\sigma = 0.5$ correspond to all systems where the self-assembly process is inhibited (*i.e.*, overall neutral particles irrespective of the confinement type): particles bond to the substrate, but they do not aggregate. For nonaggregated systems under loose confinement conditions, nonzero values of $\rho(z)$ can be observed at $z \approx 1.5$ (in units of 2σ), but such values are negligible in comparison to the values of $\rho(z)$ at $z/2\sigma = 0.5$. On the other hand, when $Z_wZ_p < 0$ and aggregation occurs, the density profiles are not peaked in proximity of the bottom wall but rather close to the center of the box size along the z-direction. In these cases though, the $\rho(z)$ curves are not symmetric with respect to $z \approx L_z/2$ but are slightly shifted toward the top wall, meaning that the aggregates tend to float above the charged substrate.

It is also worth noting that the visual inspection of the investigated systems under loose confinement did not show any significant difference in the size nor in the morphology of the planar aggregates as compared to the corresponding cases under tight confinement.

CONCLUSION

In the present work, heterogeneously charged particles, referred to as inverse patchy colloids (IPCs), have been considered in a restricted, quasi-two-dimensional geometry. Specifically, we have focused on IPCs with an axially symmetric surface charge distribution, due to the presence of two polar patches of identical charge and an equatorial region of opposite charge on the particle surface. A selection of several IPCs with two patches has been made in order to investigate the role of both the overall particle charge and the patch size on the self-assembly process. The selected IPC systems have been confined between two parallel walls; the wall separation was varied between 1.45σ with σ being the particle diameter (tight confinement) and 2σ (loose confinement); in the first case, particles were prevented from sitting on top of each other, while in the latter case, they could possibly do it. The cases corresponding to a purely steric particle–wall repulsion were considered as reference states.

The effect of a charged bottom wall on the aggregation was investigated when the wall and the patches were carrying either like or unlike charges. The self-assembly of the selected IPC systems under confinement was investigated in conditions such that the characteristic energy of the directional attractive interactions was much greater than the thermal energy.

For purely steric particle−wall interactions, a general tendency toward the formation of planar aggregates has been observed. Our work has shown that, as soon as IPCs formed interparticle bonds, their orientational vectors lie almost in the same plane—irrespective of the patch size and the overall particle charge—even though they could freely rotate in space. Moreover, even under loose confinement conditions, no aggregation has been observed along the direction perpendicular to the plane defined by the average particle orientation. In conclusion, the investigated IPC systems always formed quasi-two-dimensional structures when confined between neutral walls.

For the almost planar structures observed between neutral walls, two different aggregation scenarios have been identified: the formation of a gel structure consisting of disordered aggregates and, in contrast, the self-assembly of a branched network purely consisting of crystalline domains; this latter structure is a novel, hybrid form of macroscopic self-aggregation, which we have termed microcrystalline gel. Similar structures have been only observed in the bulk of colloidal systems with competing short-range attractions and long-range repulsions.[30,32] The crucial parameter driving the self-assembly into ordered domains, as opposed to disordered aggregates, was proven to be the patch extension: bigger patches were found to give rise to extended structures consisting of ordered triangular domains; in contrast, smaller patches were shown to favor the formation of several ring-like particle arrangements, which consequently led to the formation of an open gel network. It is also worth noting that for IPCs with relatively smaller patches bonding contacts occur between only one patch and one equator, whereas for IPCs with bigger patches, one patch often overlaps with two neighboring equators. Surprisingly, the effect of the overall particle charge, which is responsible for the specific interplay between directional attractive and repulsive interactions, turned out to be negligible. A clear distinction based only on the patch size can therefore be made between systems which tend to form crystalline domains and systems which do not. For IPCs with relatively big patches, already trimers and quadrimers have a three-fold particle arrangement and thus they are able to act as building blocks for the formation of the microcrystalline gel. In contrast, for IPCs with smaller patches, the competition between different ring-like particle arrangements prevents assembly *via* monomer by monomer addition. In this context, it is worth noting that recently it was shown that, for a minimal protein model in two dimensions, the self-assembly *via* the sequential addition of individual monomers to a larger structure is more efficient than hierarchical processes.[33]

Since, in the investigated regime of moderate asymmetries between the charges involved in the model, the directional particle−particle repulsion was shown to play a minor role as compared to the directional interparticle attraction, the selected IPC systems between neutral walls might be associated with a specific conventional patchy system. Bonding patterns similar to those observed in the present work might in fact form also with colloids carrying two types of patches, two opposite polar patches of type A and one equatorial patch of type B, such that only AB bonds are possible. Nonetheless, for conventional patchy particles of this type, the tendency to form planar structures under loose confinement conditions is not guaranteed as it is for IPC systems where the particle−particle repulsion disfavors the assembly along the direction perpendicular to the particle plane. It is possible to speculate that a bulk phase consisting of parallel planar layers might be feasible at least for those IPC systems where microcrystalline gels form; in contrast for IPCs systems where a disordered gel network is formed, the competition between local arrangements with different ring-like coordination might disfavor the assembly of planar aggregates in the bulk.

As soon as charge was assigned to the substrate, the self-assembly scenario of the IPCs became more complex. As a consequence of the competition between the particle−particle and the particle−wall interaction energies, we have observed either the formation of extended structures or the complete inhibition of the aggregation process. When the bottom wall and the patches carried charges of opposite sign, the overall particle charge turned out to be the key parameter to control the aggregation properties of the systems: overall charged particles formed gel structures (either disordered or microcrystalline according to the patch size), while overall neutral particles did not aggregate at all but rather were adsorbed to the substrate monomer by monomer. When the bottom wall and the patches carried charges of the same sign, aggregation of extended structures was observed; however, due to the strong adsorption of the particles to the substrate, the aggregates were found to be smaller and more elongated in comparison to those formed by the corresponding IPCs confined between neutral walls. Moreover, in IPC systems that formed microcrystalline gels, the presence of a bottom wall such that particles are favored to orient themselves parallel to it affected the internal structure of the aggregates: as a consequence of the competition between particle−particle and particle−wall bond formation, locally disordered domains were found together with crystalline domains within the same gel network. Optimal self-assembly in

the sense of "pure structures" and larger domains was thus found to occur in the presence of neutral walls.

The present work forms the basis for the investigation of the collective behavior of heterogeneously charged colloids close to confining and possibly charged walls. For systems consisting of quadrupolar IPCs with two patches, three characteristic parameters, namely, the patch extension, the overall particle charge, and the charge of the substrate, have been varied within moderate regimes. Sampling of the parameter space beyond the chosen ranges as well as the introduction of additional parameters, such as variable screening conditions, different numbers of patches per particle and patterned substrates represent possible future steps. It is worth noting that our model features a strong anisotropy in the interactions but no anisotropy in the particle shape. Though the major effects described here are arising from the anisotropy in the interactions and thus small deviations of the real particles from sphericity are not anticipated to have dramatic effects, the combination of shape asphericity and anisotropic interactions is to be addressed in the future.

The presented results suggest various applications of confinement directed self-assembly of (nano) colloids (or proteins) on substrates, where the assembly patterns can be modified *in situ via* the pH, which controls the charges on the patches, on the equatorial regions of the particles and on the substrate depending on the respective isoelectric points. By changing the salinity, it is moreover possible to tune the interaction range of the screened Coulomb interactions.

TABLE 1. Maximum/Minimum Interaction Energies of Characteristic Reference Configurations for Each IPC Type[a]

IPC type	$\varepsilon_{PP}/\lvert\varepsilon_{EP}\rvert$	$\varepsilon_{EE}/\lvert\varepsilon_{EP}\rvert$	$\varepsilon_{PW}/\lvert\varepsilon_{EP}\rvert$	$\varepsilon_{EW}/\lvert\varepsilon_{EP}\rvert$
30n	5.09898403	0.05869047	±4.64682970	±1.67603214
30c	0.16974171	0.12147218	±0.15989868	±1.86408675
45n	4.08059184	0.11726397	±4.37617824	±1.87726070
45c	0.24698159	0.20549022	±0.27764452	±2.19682136

[a] For sake of clarity, the reference configurations are graphically reproduced in panels a and c of Figure 1 together with their corresponding acronym. The second and the third columns of the table refer to the particle−particle interaction between two particles at contact (*i.e.*, $r/2\sigma = 1$): ε_{EE} and ε_{PP} are the maximum values of the repulsion in the equatorial−equatorial and polar−polar configuration, respectively, while ε_{EP} is the minimum interaction energy corresponding to the equatorial−polar configuration. The latter value corresponds to the energy unit, *i.e.*, $\varepsilon_{EP} = -1$. The fourth and the fifth columns of the table refer to the particle−wall interaction for a particle located at distance $r/2\sigma = 0.5$ from the wall: ε_{PW} and ε_{EW} are the energy values corresponding to the polar−wall and equatorial−wall configuration, respectively. The positive signs in front of the reported values correspond to a wall charge such that $Z_wZ_p > 0$, while the negative signs correspond to the opposite case. The two bottom rows of the table correspond to the cases that are graphically represented in Figure 1.

MODEL AND METHODS

We considered several inverse patchy colloid (IPC) systems confined in a quasi-two-dimensional geometry and performed Monte Carlo simulations in the canonical ensemble for a selected state point.

Particle−Particle Interaction. The coarse-grained model put forward in ref 19 features a spherical, impenetrable colloidal particle (of radius σ and central charge Z_c) carrying two interaction sites (each of charge Z_p) located at a distance e ($<\sigma$) in opposite directions from the particle center. The electrostatic screening conditions (expressed *via* the Debye screening length κ^{-1}) determine the range δ of the pair interaction independently of the relative orientation of the particles. For each set (σ,e,δ), the patch size, defined by the opening angle γ, is uniquely determined by eqs 10 and 11 of ref 19. All lengths are expressed in units of the particle diameter (*i.e.*, $2\sigma = 1$). We fixed the interaction range $\delta = 0.2$ (corresponding to $\kappa\sigma = 5$ with the choice $\kappa\delta = 2$) and focused on two different patch extensions, namely, $\gamma \approx 30°$ and $\approx 45°$ (corresponding to $e = 0.32$ and 0.22, respectively). The energy strengths appearing in eq 13 of ref 19 are set by mapping (with the so-called "max" scheme) the coarse-grained potential to the analytical Debye−Hückel potential developed for IPCs in water at room temperature.[19] The coarse-grained pair potential is further normalized such that the minimum of the equatorial−polar attraction sets the energy unit. Going beyond ref 19, we considered not only overall neutral particles (*i.e.*, $Z_{tot} = Z_c + 2Z_p = 0$) but also overall charged units with $|Z_c/2Z_p| > 1$; that is, the net charge is of the same sign as Z_c. A nonzero overall particle charge results into a different interplay between the directional attractive and repulsive contributions to the interparticle effective potential. We selected four different IPC types, and we labeled them γi, where $\gamma = 30,45$ represents the patch extension in degrees, while $i = n,c$ refers to the overall particle charge. In both cases of overall charged particles, Z_{tot} has been chosen such that the equatorial−equatorial repulsion is comparable to the polar−polar repulsion; specifically, $Z_{tot} = -10/9Z_p$ for system 30c, while $Z_{tot} = -4/9Z_p$ for system 45c. Columns 2 and 3 of Table 1 report the resulting particle−particle interaction energies at contact for each of the IPC types; additionally, in panel b of Figure 1, the pair potentials for systems 45n and 45c are displayed.

Particle−Wall Interaction. The interaction between a coarse-grained IPC and a neutral wall perpendicular to the z-axis is a steric interaction modeled as a hard repulsion taking place when the particle is located at distance $z \le \sigma$ from the wall. In the presence of a charged wall with surface charge $\sigma_w = Z_w/4\sigma^2$, a screened electrostatic interaction must be added to the particle−wall hard repulsion. The electrostatic interaction has been modeled *via* a mapping scheme, outlined in the following, that is consistent with the particle−particle potential description developed in ref 19. Within the Debye−Hückel approximation, the external field generated by a uniformly charged plane perpendicular to the z-axis is[34]

$$\Phi(z) = \frac{2\pi\sigma_w}{\kappa\varepsilon}\exp[\kappa(\sigma - z)] \quad (1)$$

where z is the distance between the particle center and the wall; the minimum particle−wall distance is $z = \sigma$ because of the hard sphere constraint. In eq 1, the Debye screening length κ^{-1} and the dielectric permittivity ε are the same as in the particle−particle interaction potential.[19] The potential energy of an IPC in the presence of the external field $\Phi(z)$ can be expressed as[35]

$$\Psi(z,\theta) = Q_{eff}(\theta)\Phi(z) \quad (2)$$

where $Q_{eff}(\theta)$ is the orientational dependent, effective charge of an IPC; $Q_{eff}(\theta)$ can be read off from eqs 3 and 4 of ref 19 as

$$Q_{eff}(\theta) = \frac{\exp(\kappa\sigma)}{(1+\kappa\sigma)} \times \left[Z_cq_e + 2Z_pq_e\sum_{l=1}^{\infty}\left(\frac{a}{\sigma}\right)^{2l}(4l+1)P_{2l}(\cos\theta)\right] \quad (3)$$

where q_e is the magnitude of the elementary charge, $a \equiv e$, θ is the angle with respect to the z-axis, and $P_{2l}(\cos\theta)$ is the Legendre polynomial of order $2l$. Since our coarse-grained particle model features two types of interaction spheres—one big (B) central sphere, corresponding to the interaction sphere of the bare colloid, and two small (S) out-of-center spheres, corresponding to the interaction spheres of the patches[19]—the coarse-grained particle−wall potential can be written as the sum of two contributions. Each contribution is factorized into an energy strength and a geometrical factor, as postulated also in the derivation of the coarse-grained particle−particle description.[19] Specifically, within the interaction range set by the screening conditions (*i.e.*, $\sigma \le z \le \sigma + \delta$), the particle−wall interaction can be written as

$$U(z,\theta) = w_{SW}(z,\theta)u_{SW} + w_{BW}(z,\theta)u_{BW} \quad (4)$$

where u_{SW} and u_{BW} are the energy strengths to be determined *via* the mapping with the analytical potential in eq 2, while $w_{\alpha W}$ are dimensionless weight factors which depend on the distance and the relative orientation between the IPC and the wall. The weight factors $w_{\alpha W}$ are proportional to the total overlap volume between the planar wall and all the interaction spheres α contributing to the specific αW interaction

$$w_{\alpha W} = \Omega_{O_T}^{\alpha W}/\Omega_R \quad (5)$$

where $\Omega_{O_T}^{BW} = \pi/3(R_B - z)(2R_B^2 - z^2 - R_B z)$ with $R_B = (\sigma + \delta)$, while $\Omega_{O_T}^{SW} = \pi/3\sum_{i=1}^{2}(R_S - z_i)(2R_S^2 - z_i^2 - R_S z_i)$ with $R_S = (\sigma + \delta - e)$ and z_i being the distance of patch i from the wall; $\Omega_R = 4\pi\sigma^3/3$ is the reference volume. Two characteristic configurations, namely, the polar−wall and the equatorial−wall configuration (reproduced in panel c Figure 1 for sake of clarity), are needed to evaluate the yet undefined energy strengths of the coarse-grained particle−wall interaction. Once the mapping with the analytical description is performed, the coarse-grained particle−wall interaction is fully consistent with the particle−particle coarse-grained description. The particle−wall potential is further normalized in units of $|\varepsilon_{EP}|$. We considered walls that carry a surface charge with either the same sign as the patches (*i.e.*, $Z_w Z_p > 0$) as well as the same sign as the bare colloid (*i.e.*, $Z_w Z_p < 0$). The specific values of the wall charge have been chosen such that, when $Z_w Z_p > 0$, the corresponding minima of the particle−wall attraction of all of the selected IPC types are comparable to each other, being at the same time also comparable to the particle−particle bonding energy. Specifically, $Z_w = \pm 1/3 Z_p$ for systems 30n and 30c, while $Z_w = \pm 1/9 Z_p$ for systems 45n and 45c. For σ values ranging from tens of nanometers to some micrometers,[19] the chosen σ_w values are well below one elementary charge per 60 Å^2.[36] Columns 4 and 5 of Table 1 report the resulting typical particle−wall interaction energies at contact for each IPC type; additionally, panel d of Figure 1 reports the particle−wall potentials for systems 45n and 45c in the presence of a wall carrying a surface charge such that $Z_w Z_p > 0$.

Monte Carlo Simulations. We considered selected IPC systems confined in a quasi-two-dimensional geometry by means of two planar walls both perpendicular to the z-axis. The top wall of the sample was always neutral, while the bottom wall could be neutral or charged. We performed Monte Carlo (MC) simulations in the canonical ensemble at $T^* = 0.10$ (temperature in reduced units, *i.e.*, $T^* = k_B T/|\varepsilon_{EP}|$); we considered $N = 1000$ particles in a volume $V = L_x L_y L_z$, where $L_x/2\sigma = L_y/2\sigma = 50$ and $L_z/2\sigma = 1.45$ or $L_z/2\sigma = 2$. In the case of tight confinement (*i.e.*, $L_z/2\sigma = 1.45$), particles were prevented from sitting on top of each other, while in the case of loose confinement (*i.e.*, $L_z/2\sigma = 2$), the box size possibly allowed two particles at contact to pile up along the z-axis. Each MC step consists on average of N trial particle moves, where the acceptance rule is given by the Metropolis criterion. A particle move is defined as both a displacement in each direction of a random quantity distributed uniformly between $\pm\delta r$ as well as a rotation around a random axis of a random angle distributed uniformly between $\pm\delta\theta$. The chosen values for the trial changes are $\delta r = 0.05$ and $\delta\theta = \delta r/2\sigma$ rad. Since the aggregation process was studied out of equilibrium, we ran for each IPC type 10 MC runs in parallel starting from different initial conditions. Each run lasted for a total of 10^7 MC steps. All quantities shown in this paper are averages over the final 10^3 MC steps, corresponding to 100 different configurations per independent run.

Conflict of Interest: The authors declare no competing financial interest.

Acknowledgment. Financial support by the Austrian Science Foundation (FWF) under Project Nos. M1170-N16, V249-N27, P23910-N16, and F41 (SFB ViCoM) is gratefully acknowledged.

REFERENCES AND NOTES

1. Juhl, S. B.; Chan, E. P.; Ha, Y.-H.; Maldovan, M.; Brunton, J.; Ward, V.; Dokland, T.; Kalmakoff, J.; Farmer, B.; Thomas, E. L.; *et al.* Assembly of Wiseana Iridovirus: Viruses for Colloidal Photonic Crystals. *Adv. Funct. Mater.* **2006**, *16*, 1086–1094.
2. Daniel, M. C.; Tsvetkova, I. B.; Quinkert, Z. T.; Murali, A.; De, M.; Rotello, V. M.; Kao, C. C.; Dragnea, B. Role of Surface Charge Density in Nanoparticle-Templated Assembly of Bromovirus Protein Cages. *ACS Nano* **2010**, *4*, 3853–3860.
3. Lopez, C. Materials Aspects of Photonic Crystals. *Adv. Mater.* **2003**, *15*, 1679–1704.
4. Horejs, C.; Gollner, H.; Pum, D.; Sleytr, U. B.; Peterlik, H.; Jungbauer, A.; Tscheliessnig, R. Atomistic Structure of Monomolecular Surface Layer Self-Assemblies: Toward Functionalized Nanostructures. *ACS Nano* **2011**, *5*, 2288–2297.
5. Ruzicka, B.; Zaccarelli, E.; Zulian, L.; Angelini, R.; Sztucki, M.; Moussaïd, A.; Narayanan, T.; Sciortino, F. Observation of Empty Liquids and Equilibrium Gels in a Colloidal Clay. *Nat. Mater.* **2011**, *10*, 56–60.
6. van Blaaderen, A. Materials Science: Colloids Get Complex. *Nature* **2006**, *439*, 545–546.
7. Bianchi, E.; Blaak, R.; Likos, C. N. Patchy Colloids: State of the Art and Perspectives. *Phys. Chem. Chem. Phys.* **2011**, *13*, 6397–6410.
8. Pawar, A. B.; Kretzschmar, I. Fabrication, Assembly, and Application of Patchy Particles. *Macromol. Rapid Commun.* **2010**, *31*, 150–168.
9. Wang, Y.; Wang, Y.; Breed, D. R.; Manoharan, V. N.; Feng, L.; Hollingsworth, A. D.; Weck, M.; Pine, D. J. Colloids with Valence and Specific Directional Bonding. *Nature* **2012**, *491*, 51–55.
10. Glotzer, S. C.; Solomon, M. J. Anisotropy of Building Blocks and Their Assembly into Complex Structures. *Nat. Mater.* **2007**, *6*, 557–562.
11. Haji-Akbari, A.; Engel, M.; Keys, A. S.; Zheng, X.; Petschek, R. G.; Palffy-Muhoray, P.; Glotzer, S. C. Disordered, Quasicrystalline and Crystalline Phases of Densely Packed Tetrahedra. *Nature* **2009**, *462*, 773–777.
12. Sacanna, S.; Pine, D. J. Shape-Anisotropic Colloids: Building Blocks for Complex Assemblies. *Curr. Opin. Colloid Interface Sci.* **2011**, *16*, 96–105.
13. Chen, Q.; Bae, S. C.; Granick, S. Directed Self-Assembly of a Colloidal Kagome Lattice. *Nature* **2011**, *469*, 381–384.
14. Jones, M. R.; Mirkin, C. A. Self-Assembly Gets New Direction. *Nature* **2012**, *491*, 42–43.
15. Damasceno, P. F.; Engel, M.; Glotzer, S. C.; Chen, Q.; Bae, S. C.; Granick, S. Predictive Self-Assembly of Polyhedra into Complex Structures. *Science* **2012**, *337*, 453–457.
16. Hong, L.; Cacciuto, A.; Luijten, E.; Granick, S. Clusters of Amphiphilic Colloid Spheres. *Langmuir* **2008**, *24*, 621–625.
17. Zhang, F.; Skoda, M. W. A.; Jacobs, R. M. J.; Zorn, S.; Martin, R. A.; Martin, C. M.; Clark, G. F.; Weggler, S.; Hildebrandt, A.; Kohlbacher, O.; *et al.* Reentrant Condensation of Proteins in Solution Induced by Multivalent Counterions. *Phys. Rev. Lett.* **2008**, *101*, 148101.
18. Zhang, F.; Roth, R.; Wolf, M.; Roosen-Runge, F.; Skoda, M. W. A.; Jacobs, R. M. J.; Stzucki, M.; Schreiber, F. Charge-Controlled Metastable Liquid−Liquid Phase Separation in Protein Solutions as a Universal Pathway towards Crystallization. *Soft Matter* **2012**, *8*, 1313–1316.
19. Bianchi, E.; Kahl, G.; Likos, C. N. Inverse Patchy Colloids: From Microscopic Description to Mesoscopic Coarse-Graining. *Soft Matter* **2011**, *7*, 8313–8323.

20. Verwey, E. J. W.; Overbeek, J. T. G. *Theory of the Stability of Lyophobic Colloids*; Elsevier: Amsterdam, 1948.
21. Bozic, A. L.; Podgornik, R. Symmetry Effects in Electrostatic Interactions between Two Arbitrarily Charged Spherical Shells in the Debye–Hückel Approximation. *J. Chem. Phys.* **2013**, *138*, 074902.
22. Kretzschmar, I.; Song, J. H. Surface-Anisotropic Spherical Colloids in Geometric and Field Confinement. *Curr. Opin. Colloid Interface Sci.* **2011**, *16*, 84–95.
23. Whitelam, S. Control of Pathways and Yields of Protein Crystallization through the Interplay of Nonspecific and Specific Attractions. *Phys. Rev. Lett.* **2010**, *105*, 088102.
24. Geyer, T.; Born, P.; Kraus, T. Switching between Crystallization and Amorphous Agglomeration of Alkyl Thiol-Coated Gold Nanoparticles. *Phys. Rev. Lett.* **2012**, *109*, 128302.
25. Workum, K. V.; Douglas, J. F. Symmetry, Equivalence, and Molecular Self-assembly. *Phys. Rev. E* **2006**, *73*, 031502.
26. Weddemann, A.; Wittbracht, F.; Eickenberg, B.; Hütten, A. Magnetic Field Induced Assembly of Highly Ordered Two-Dimensional Particle Arrays. *Langmuir* **2010**, *26*, 19225–19229.
27. Osterman, N.; Babič, D.; Poberaj, I.; Dobnikar, J.; Ziherl, P. Observation of Condensed Phases of Quasiplanar Core-Softened Colloids. *Phys. Rev. Lett.* **2007**, *99*, 248301.
28. Leunissen, M. E.; Vutukuri, H. R.; van Blaaderen, A. Directing Colloidal Self-Assembly with Biaxial Electric Fields. *Adv. Mater.* **2009**, *21*, 3116–3120.
29. Schmidle, H.; Jäger, S.; Hall, C. K.; Velev, O. D.; Klapp, S. H. L. Two-Dimensional Colloidal Networks Induced by a Uni-axial External Field. *Soft Matter* **2013**, *9*, 2518–2524.
30. Zhang, T. H.; Groenewold, J.; Kegel, W. K. Observation of a Microcrystalline Gel in Colloids with Competing Interactions. *Phys. Chem. Chem. Phys.* **2009**, *11*, 10827–10830.
31. Svab, E.; Hiltunen, E. J. Medium Range Order from Total and Partial Pair Correlation Functions of Metallic Glasses. *Phys. Scr.* **1992**, *46*, 185–188.
32. Zhang, T. H.; Klok, J.; Tromp, R. H.; Groenewold, J.; Kegel, W. K. Non-equilibrium Cluster States in Colloids with Competing Interactions. *Soft Matter* **2012**, *8*, 667–672.
33. Haxton, T. K.; Whitelam, S. Do Hierarchical Structures Assemble Best *via* Hierarchical Pathways? *Soft Matter* **2013**, DOI: 10.1039/C3SM27637F.
34. Russel, W. B.; Saville, D. A.; Schowalter, W. R. *Colloidal Dispersions*; Cambridge University Press: New York, 1995.
35. Jackson, J. D. *Classical Electrodynamics*, 3rd ed.; Wiley: New York, 1999.
36. Konieczny, M.; Likos, C. N. From Sea-Urchins to Starfishes: Controlling the Adsorption of Star-Branched Polyelectrolytes on Charged Walls. *Soft Matter* **2007**, *3*, 1130–1134.